OPTIMAL DEPLOYMENT SCHEDULE FOR VIBRATION REDUCTION OF LIFT-OFFSET COAXIAL ROTORCRAFT USING INDIVIDUAL BLADE CONTROL

Seong Hyun Hong, Dept. of Aerospace Eng., Konkuk University, Seoul 05029, South Korea
Dong Kyun Kim, Dept. of Aerospace Eng., Konkuk University, Seoul 05029, South Korea
Sung Nam Jung, School of Mechanical and Aerospace Eng., Konkuk University, Seoul 05029, South Korea

Abstract

This study investigates the optimal vibration reduction using the IBC (Individual Blade Control) actuation concept for a coaxial lift-offset (L.O.) rotorcraft in high-speed cruise flight. The rotorcraft vibration analysis model consists of a three-bladed coaxial rotor and a one-dimensional (1D) finite element (FE) fuselage stick model. A 1D FE stick model of the fuselage is constructed based on the natural frequency data of XH-59A and several other conventional helicopters. A total of 14 free vibrating modes are used to describe the air-frame motions, after conducting a convergence study on the vibration behavior of the vehicle. The rotor-body vibration analysis is carried out using either one-way or two-way coupled method, and the results are validated with XH-59A flight test data. The two-way coupled predictions show relatively good correlations with the flight test data. The active vibration reduction gains obtained at the rotor hub and the pilot-seat via various actuation scenarios are examined. The IBC actuation is demonstrated to be very effective in reducing the vibration levels at both the locations of the vehicle. A multi-harmonic IBC actuation schedule enables to suppress the overall vehicle vibration by 80.6%, as compared to the baseline uncontrolled case.

1. INTRODUCTION

High levels of vibration, large noise emissions, and relatively poor aerodynamic efficiencies are some of the major concerns in modern rotorcraft applications. The problem becomes aggravated with increases in flight speeds as the edgewise rotor experiences greater differences in incoming air velocities between the advancing and retreating sides of the rotor. Many innovative ideas have been devised to overcome the shortcomings in relation to the speed barriers of helicopter flights. One prominent concept is to apply the L.O. mechanism with which the lift generation capacity of the rotor is maximized without compromising the aerodynamic deficiencies in the retreating side of the rotor. The roll moment equilibrium is satisfied with the lift produced by a pair of coaxial, counter-rotating rotors that operate with equal and opposite roll moments. The XH-59A is the first aircraft to successfully demonstrate the L.O. concept, achieving the maximum forward speed of 240 knots in level cruise mode (Refs. 1-2). However, the test program was terminated due to severe vibrations and high fuel consumption met in the flight.

To analyze the problem closely, precise modeling of the main rotor and the fuselage system, considering their interactional behavior, is crucial for reliable vibration prediction of a full rotorcraft, especially at the cockpit location. The rotor-body coupled vibration analysis can be performed using either approach: one-way or two-way coupling. The former considers the main rotor and the fuselage system separately: the isolated rotor computes the vibratory hub loads and then applies the load spectrum to excite the fuselage (from the hub) for evaluating the vibration at the desired stations of the fuselage. The process is unilateral, with no interactions in between. In the latter method, however, they interact with each other, in which the vibratory loads produced by the rotor are transferred to the fuselage, which in turn changes the motion of the hub by the dynamic response of the fuselage. The changed hub motions (body) modify the hub loads (rotor) accordingly. These interactions are repeated until substantial convergence within a tolerance is reached. Considering the inherent coupling of the problem, the latter approach is thought to be more general for a realistic evaluation of rotor-body vibration response. Nonetheless, there is a need to systematically evaluate the difference in accuracy and efficacy between the two approaches.

The interaction between the rotor and the fuselage affects the vibration for both the rotating and non-rotating system of a rotorcraft. Previous studies have mostly focused on the rotor-body coupling for conventional helicopters (Refs. 3-5), while the L.O. rotor system has been analyzed using the rotor in isolation or with a simplified fuselage model (Refs. 6-13). So far, a comprehensive study on the loads and vibration behavior of L.O. coaxial rotorcraft, considering the whole rotorcraft system, has not been covered much in the literature. A few exceptions are: Blackwell and Millott (Ref. 14), and Lee et al (Ref. 15). Blackwell and Millot (Ref. 14) developed a FE model of a L.O. coaxial compound helicopter with a fuselage and active vibration control system (AVCS) installed at the non-rotating system. They successfully demonstrated the vibration reduction of X2TD, which was developed based on the earlier platform of XH-59A rotor. Lee et al. (Ref. 15) modeled the fuselage using a 1D FE stick model along with a one-way coupling approach for vibration reduction of XH-59A with the application of IBC and AVCS. Considerable vibration reduction gains were reported to be obtained, with the co-actuation at both rotor (IBC) and fuselage (AVCS). However, the vibratory hub load is not considered with coupled fuselage effect. Despite the recent attempts, there still remains to fill the gap in the literature in relating to the rotor-body coupled vibration analysis of the L.O. coaxial rotorcraft system, especially including application of the two-way coupling approach.

The objectives of the present study are threefold: 1) assessing the accuracy and efficiency of the rotor-body coupled vibration predictions obtained between the one-way and two-way coupling methods in reference to XH-59A flight test data in high-speed cruise condition; 2) identifying the coupled vibration behavior of the rotor and fuselage; and 3) finding the best actuation scenario for the minimum vibration using the IBC scheme.

2. SOLUTION APPROACHES

2.1. Fuselage FE model

Table 1 shows the summary of the general properties of XH-59A (Ref. 1), which is a 3-bladed coaxial rotor with 5.48 m long and a vehicle weight of 5,398 kg. For the vibration analysis, the fuselage dynamic model is first constructed using MSC.NASTRAN. Modeling the fuselage varies from a simple 1D FE stick model to a detailed 3D FE model. For both the efficiency and convenience purpose, a simple 1D FE stick model is adapted to account for the dynamic motions of the fuselage (Ref. 4). Since most of the normal mode characteristics of the XH-59A fuselage are not publicly available, except the first fuselage symmetric bending mode (Ref. 1), values taken from conventional helicopters (e.g. UH-60A, AH-1G, BO-105) are adopted instead for the target modes of the fuselage (Refs. 16-18). The target frequencies of the fundamental modes of the fuselage is given in Table 2. The cross-sectional dimension and structural properties of each beam element in the stick model are appropriately assumed and varied to match the target frequencies set for the fuselage structure. The overall vehicle weight and CG location of the XH-59A are held constant during the frequency tuning (Ref. 19). Fig. 1 illustrates the final 1D FE stick model built for the present XH-59A fuselage, which consists of 37 elastic beam FE's, 20 concentrated masses, and a flexible pylon that creates the physical connection between the rotor shaft and the fuselage. The 1D FE stick model includes the flexible pylon mounting system, modeled to match the normal modes of the fuselage. Five multipoint constraints using RBE2 element are used to simulate elastomeric mounting system, with one bar element installed to model the lift link of the rotor shaft mounting system (Ref. 18). It is noted that the lift link is the primary load path of the vertical force carried through the upper and lower rotor.

2.2. Rotor-body coupled analysis

Fig. 1 shows the schematic view of the between the one-way and two-way rotor-body coupled vibration analysis methodologies. The one-way coupling analysis is mainly conducted in MSC.NASTRAN using the direct frequency response analysis solution (SOL 108). The vibratory hub load spectrum obtained from the isolated rotor system with blade passage frequencies (BPF), which is 3 per rotor revolution (3P), are directly applied to the upper and lower hub positions, as indicated in Fig. 1. The structural response of the fuselage is then computed as discrete excitation frequencies in direct response analysis by solving a set of coupled matrix equations of the system. To this purpose, a ground vibration analysis model of the XH-59A fuselage is constructed, using the same set of normal modes as the aforementioned 1D FE stick model, which including the bungee cables connected to the upper rotor hub and at the empennage as depicted in Fig. 2 (Ref. 15).

The two-way coupling analysis is conducted using the comprehensive dynamics analysis code CAMRAD II (Ref. 20). The rotor-body coupled analysis is performed through the interactions between the hub and airframe motion. To consider the elasticity of the fuselage, the motion loop option in CAMRAD II is used during the vehicle trim process. Fig. 3 illustrates the flow diagram of the analysis process. The trim loop consists of the motion loop itself, which iteratively computes the effect of hub loads on the vehicle motion sensors. To avoid harmonic coupling between the rotor and airframe, the solution is conducted in nonrotating frame. The elasticity of the fuselage is converted to generalized mass, natural frequency, and eigenvectors from the normal modes analysis results of 1D FE stick model. The interactions are computed at three collocation points, called motion sensors, as depicted in Fig. 1, which capture the elastic behavior of the fuselage. The motion sensors are positioned at the lower and upper rotor hub, and the pilot seat. The rotor hub locations are chosen since they are directly connected to the rotor, which is the main source of the vibration. The fuselage motion is calculated using the linear and angular mode shapes of the respective motion sensor, considering all the forces and moments acting on the rotorcraft.

The governing equation of motion of a rotor-body coupled system is expressed as:

(1) $$\ddot{\mathbf{r}} + 2\boldsymbol{\zeta}\boldsymbol{\omega}\dot{\mathbf{r}} + \boldsymbol{\omega}^2\mathbf{r} = \mathbf{f}$$

where $\mathbf{r}$ is the modal degree of freedom (DOF) in generalized coordinates, $\boldsymbol{\zeta}$ and $\boldsymbol{\omega}$ are the critical damping ratio and the natural frequency of the normal mode, respectively, and $\mathbf{f}$ is the excitation force in generalized coordinates defined as:

(2a) $$\mathbf{f} = \mathbf{S}^{\mathrm{T}}\mathbf{F}$$

(2b) $$\mathbf{S}^{\mathrm{T}} = \lfloor u_X \quad u_Y \quad u_Z \quad \phi_X \quad \phi_Y \quad \phi_Z \rfloor$$
$$\mathbf{F}^{\mathrm{T}} = \lfloor F_X \quad F_Y \quad F_Z \quad M_X \quad M_Y \quad M_Z \rfloor$$

where $\mathbf{S}$ is the mode shape vector of the linear and angular mode shapes and $\mathbf{F}$ is the vibratory hub loads in non-rotating frame, respectively. Since 1D FE fuselage model includes the rotor as a concentrated mass at the hub center, the inertial loads are included twice in the two-way rotor-body coupled analysis (Ref. 21). Therefore, the inertial loads must be eliminated from the generalized force array. The inertial loads are calculated as the mass (hub and blade) multiplied by the acceleration of the hub. The fuselage excitation force is expressed as:

(3) $$\mathbf{F} = \mathbf{F}_{\mathrm{LH}} + \mathbf{F}_{\mathrm{UH}} + \mathbf{M}_{\mathrm{LH}}\mathbf{S}_{\mathrm{LH}}\ddot{\mathbf{r}} + \mathbf{M}_{\mathrm{UH}}\mathbf{S}_{\mathrm{UH}}\ddot{\mathbf{r}}$$

where the subscripts LH and UH designate the lower rotor hub and upper rotor hub, respectively, and $\mathbf{M}$ denotes the mass matrix. The final form of governing equation is given by:

(4) $$(\mathbf{I} - \mathbf{S}_{\mathrm{LH}}^{\mathrm{T}}\mathbf{M}_{\mathrm{LH}}\mathbf{S}_{\mathrm{LH}} - \mathbf{S}_{\mathrm{UH}}^{\mathrm{T}}\mathbf{M}_{\mathrm{UH}}\mathbf{S}_{\mathrm{UH}})\ddot{\mathbf{r}} + 2\boldsymbol{\zeta}\boldsymbol{\omega}\dot{\mathbf{r}} + \boldsymbol{\omega}^2\mathbf{r}$$
$$= \mathbf{S}_{\mathrm{LH}}^{\mathrm{T}}\mathbf{F}_{\mathrm{LH}} + \mathbf{S}_{\mathrm{UH}}^{\mathrm{T}}\mathbf{F}_{\mathrm{UH}}$$

where $\mathbf{I}$ is the identity matrix. The generalized mass matrix is no longer diagonal so, the governing equation is fully coupled between the rotor and the body motions. The vibratory hub loads from the rotor are transferred to the fuselage, which changes the hub motion according to the mode shapes of the motion sensor locations on the fuselage. The modified hub motion then alters the rotor hub loads. These interactions are repeated until a converged solution is obtained. In either one-way or two-way coupling analysis, a structural damping ratio of 2% critical is used considering that its range is generally within 1 to 4% (Ref. 17).

2.3. Rotor comprehensive analysis

CAMRAD II is used to perform the rotor-body coupled vibration analysis of the XH-59A rotorcraft in high-speed cruise flight (200knots, advance ratio μ = 0.53). Fig. 4 shows the structural and aerodynamic analysis models used for the blades. The blade is discretized using 13 FE's, with one rigid element installed near the blade root. Each FE has 15 DOF, including 3 axial, 2 flap, 2 lag, and 2 elastic twist motions. A pitch link with 13,558 N/m spring constant is used to model the pitch control input while keeping the first torsion frequency of the rotor. The aerodynamic analysis is based on the ONERA-

EDLIN unsteady airfoil theory with C81 table look-up with a rolled-up tip vortex wake model. The trim analysis consists of six inputs and six targets of the counter-rotating rotor system in high-speed cruise flight. The trim variables include the mean and differential collective pitch angles of the whole rotor and the longitudinal and lateral cyclic pitch angles of each rotor. The goal is to balance the rotor system by adjusting the pitch moments of the lower and upper rotor and the difference between the lower and upper rotor hub roll moments, while matching the L.O. and the thrust of the vehicle. The L.O. is defined below, relating the lift produced by the coaxial rotor system (L) with the rotor radius (R) and differential roll moments (ΔM_x).

(5) $$\text{L.O.} = \frac{\Delta M_x}{L \cdot R}$$

To simplify the analysis, it is assumed that the fuselage aerodynamic forces balance themselves, including the rotor drag and auxiliary propulsion system. The rotor rotational speed is fixed to 98% of the nominal RPM considering the flight test results in Ref. 19. To account for the vibration level of whole aircraft, the vibration index (VI_R) of the rotor hub and body are defined in an index form by the guidelines described in the ADS-27A-SP document (Ref. 22) as:

(6) $$\text{VI}_\text{R} = \left\{ \alpha_1 \frac{\sqrt{(0.5F_X)^2 + (0.67F_Y)^2 + F_Z^2}}{W_0} + \alpha_2 \frac{\sqrt{M_X^2 + M_Y^2}}{W_0 R} \right\}$$

Where F_X, F_Y, and F_Z are the hub forces in the longitudinal, lateral, and vertical directions, respectively, and M_X, and M_Y are the rolling and pitching moments. In addition, W_0 is the vehicle weight, and α_i (i = 1,2) ($0 \le \alpha_i \le 1$) are the weighting factors, respectively. The present analysis calculates VI_R using the same weight factors (α_i = 1). Unless otherwise stated, the hub vibration is evaluated using the lowest BPF (i.e. 3P) of the three-blade rotor. The vibration index of a fuselage VI_F is defined by the accelerations evaluated at the pilot seat (MS 1) as:

(7) $$\text{VI}_\text{F} = \frac{\sqrt{a_X^2 + a_Y^2 + a_Z^2}}{g}$$

where a_X, a_Y, a_Z are the accelerations in the longitudinal, lateral, and vertical directions respectively, and g is the gravity constant, respectively. The overall aircraft vibration $VI_{overall}$ is expressed by combining Eqs. (6) and (7) into:

(8) $$\text{VI}_\text{overall} = w_1 \text{VI}_\text{R} + w_2 \text{VI}_\text{F}$$

where w_1 and w_2 denote the weighting factors ($0 \le w_i \le 1$). The present vibration analysis is carried out using the same weight factors ($w_1 = w_2 = 1$). For the performance measure, the rotor effective lift-to-drag ratio (L/D_e) is used to evaluate the efficiency of the rotor in forward flight, which is expressed as:

(9) $$L/D_e = L \cdot V / (P_i + P_0)$$

where V is the forward speed, and P_i and P_0 are the induced and profile power of the rotor, respectively.

2.4. Individual blade pitch control (IBC)

The vibratory loads of the rotor are actively suppressed using IBC actuators installed at the pitch link connected to the swashplate. The IBC pitch motions are defined by:

(10) $$T(\psi) = A_n \cos(n\psi - \Phi_n)$$

where n is the actuation frequency of harmonic control pitch input, A_n is amplitude and Φ_n is phase angle. The best actuation deployment scenario for the vibration reduction at the rotor hub and pilot seat is sought using a parametric sweep study on amplitudes, frequency, and phase angles in single harmonic actuation. Amplitude from 0° to 2.0° (increment of 0.5°) are actuated for the present study while a phase angle sweep is conducted for every 30°. Effective actuation amplitude for every actuation frequency is chosen from the parametric results to manipulate the investigation of the multiple harmonic actuations expressed as:

(11) $$T(\psi) = \sum_{n}^{N_f} A_n \cos(n\psi - \Phi_n)$$

where frequencies are added up to the frequency contents (N_f) specified by the actuation input. For the efficiency of the investigation, the phase sweep is varied by 60° with discrete amplitudes for each actuation frequency.

3. RESULTS and DISCUSSION

3.1. Validation of aeromechanics model

The structural dynamics model in the present analysis is validated first against the measured data and earlier predictions found in Refs. 1 and 2. Fig. 5 shows the comparison of the natural frequencies of XH-59A blades with the rotor speeds, obtained between the different set of results. The present predictions show good agreements on non-rotating frequencies, as compared with the measured data. It is indicated also that more close correlation is obtained with the present results than those by the earlier predictions, which confirms the correct modeling for blade structures and pitch control system of the rotor. Next, the fuselage vibration analysis model described in 1D FE stick representation is validated. Table 2 shows the summary of normal mode analysis results predicted using the 1D stick model with each of the target values set from the conventional data. It is noted that all the primary body modes are placed well within the frequency ranges specified as the targets, except the first lateral bending mode which has an error of 6.4%. In general, the frequency outcomes demonstrate the suitability of the fuselage dynamic model constructed for the rotorcraft vibration analysis. Finally, the convergence behavior of the body normal modes is investigated for the pilot seat acceleration using the two-way rotor-body coupled analysis. Fig. 6 shows the convergence results on the acceleration signals (a_X, a_Y, a_Z) computed at the pilot seat location. It is indicated that the cockpit vibration (acceleration) is quite sensitive to the vibrating modes participated in the analysis, particularly for both longitudinal and vertical vibrations (a_X and a_Z). According to the convergence study, the lowest 14 modes (up to 9P) are employed in the present coupled vibration analysis.

3.2. **Validation of rotorcraft vibration levels**

Fig. 7 shows the correlation of the results as well as the effect of the rotor-body coupling method on the cockpit vibration (a_X, a_Z) at the pilot seat with respect to the flight speeds (120 to 240 knots). The L.O. is set to 0.2 for all speeds except for 120 knots, which is 0.1. Both measured data and predicted results respectively taken from Refs. 1 and 15 are included to validate the present analysis. It is noted that Ref. 15 used the one-way rotor-body coupling, which is similar to the present one-way coupling method. Both one-way coupled predictions indicate close agreements with each other, for both acceleration signals, at flight speeds greater than 160 knots, with less satisfactory correlations at low speeds. The difference in the rolled-up free wake representations adopted in each analysis contribute to the possible source of deviations between the predictions. One thing clearly observed in Fig.7 is that the two-way rotor-body coupling significantly improves the correlation with the flight test data, in comparison with the corresponding one-way coupling method. Specifically, the longitudinal and vertical vibration levels at the pilot seat obtained using the present two-way coupling show deviations up to 8.4% as compared with the test data, at the cruise speed of 200 knots. The deviations become larger (up to 20.6%) when using the one-way coupling method. It should be remarked that the improved correlation is reached with an increase in computational costs from about 20 min to 52 min, due to the involvements of the hub reactions in the two-way coupling analysis. Based on the comparison results, the following rotor-body coupled vibration analysis is determined to be performed using the two-way coupling approach, unless otherwise specified.

Predicted results on the blade and hub loads of XH-59A rotor are investigated next. Fig. 8 shows the comparison of the blade flap bending moments (FBM) at the blade root (0.1*R*) of the upper rotor, obtained respectively from the present isolated rotor, the rotor body coupled configurations, and the flight test data, with respect to the flight speeds. As the actual L.O.s or control phase angles for each forward flight speed are not available in the public domain, so the present results are computed at the L.O. values of both 0.2 and 0.3, and presented together with the measured data. It is indicated that the present predictions with the selected L.O.'s show only a fair correlation with the test data. Though no prominent, the rotor-body coupled results slightly improves the correlation on FBM at higher flight speeds, especially with L.O. of 0.2. Fig. 9 shows the comparison of the vibratory hub pitching moments (M_Y) of the rotor obtained between the same sets of results as given in Fig. 8. The comparison results clearly indicate that the present rotor-body coupled analysis with the L.O. of 0.2 show excellent correlations with the flight test data, especially for vibratory hub pitching moments. The predicted vibratory roll moments (not shown) show less satisfactory agreements with the test data, however, the impact should be marginal due to the cancellation effect of the counter-rotating coaxial rotor system. Once again, the influence of including the fuselage on hub vibratory moments marginally improves the correlation as compared with the flight test data.

Fig. 10 illustrates the effect of the fuselage on hub vibratory forces (F_X, F_Y, F_Z) in reference to the hub vibration index (VI_R) of the rotor. it is observed that the predicted hub longitudinal forces (F_X) show a large deviation between the present analytic models (with and without the body), with differences on the other hub forces components. As reported in Ref. 23, the longitudinal force (F_X) is expected to be larger or at least comparable to the vertical force (F_Z), but no numerical values are provided. The isolated rotor analysis fails to capture this trend, while the rotor-body coupled analysis successfully reproduces it. This demonstrates the importance of considering the fuselage dynamics in predicting the vibratory hub loads. It is noted that, despite the large deviation in the longitudinal force, the changed in hub VI_R between the two methods remain small due to the increases in other load component (F_Z) as well as the scaling effect reflected in defining the index (see Eq. (6))

In Fig. 11, the rotor effective lift-to-drag ratio is validated against the flight test data at different forward speeds. Both the present results show a reasonable matches with the flight test data over the speed range. Generally, the present results with the L.O. of 0.2 indicate slightly better correlation at low speeds (below 160 knots) and follow the trend of the flight test data as the speed increases. This assumes again the relevance of using the value of 0.2 as the desired L.O. in examining the rotorcraft vibration for XH-59A rotor. Fig. 12 illustrates the free wake geometry computed using the present coaxial rotor model in high speed cruise flight. The rolled-up tip wake geometry is resolved and developed in well-organized form, indicating the sufficient convergence of the free wake model used in the present analysis.

The above validation study demonstrates that the current two-way coupled vibration methodology, trim strategy, and the detailed aeromechanics modeling are formulated correctly to yield good vibration prediction capability, not only at the rotor hub but also at the fuselage locations of the vehicle. In the subsequent sections, an active vibration reduction using IBC actuation schemes is studied for the L.O. coaxial rotorcraft. Retrimming is used throughout the rotorcraft vibration analysis.

3.3. **Vibration reduction using IBC**

A parametric sweep study is conducted to investigate the effects of single harmonic actuation with each frequency of 2P, 3P, and 4P, on the vibration response of a two-way rotor-body coupled model. The amplitudes are varied by 0.5° up to 2° half peak-to-peak (p-p) while the phase angles are swept over a rotor revolution with an interval of 30°. Fig. 13 shows the changes in the aircraft vibration ($VI_{overall}$) with different actuation frequencies. The scales in the vertical axis are kept the same between the results for a fair comparison. It is indicated that the IBC actuation due to single harmonic inputs has a significant impact on decreasing the rotor hub plus the pilot seat vibration of the vehicle. The maximum vibration reduction attains in about 67% in reference to the baseline uncontrolled case. This condition is reached at the frequency of 3P with the amplitude of 1.0° and the phase angle of 240°, as depicted in yellow circle in Fig. 13(b). As can be seen in Fig. 13, the single harmonic actuation results are straight forward to reach the minimum vibration condition. However, the multiple harmonic case is more complicated due to significant in cases in actuation scenarios with different conditions of vibratory harmonics. In order for efficiency and convenience, the best amplitudes according to each actuation frequency are selected considering the sweep study results on the single harmonic as: 2° for 2P, 1.0° for 3P and 0.5° for 4P input, respectively.

Fig. 14 shows the comparison of non-vanishing vibratory hub loads components (Fig. 14(a)) and vibration indices (Fig. 14(b), due to the application of different actuation inputs, evaluated for the coaxial L.O. rotorcraft. It is noted that the other hub loads components (e.g, F_Y, M_X, M_Z) become neglected due to the cancellation effects of the counter-rotating rotor. In Fig. 14, the baseline uncontrolled case is also included for reference purposes. It should be emphasized that each case presented in Fig. 14 represents approximately the minimum vibration conditions according to the specific actuation frequency inputs. Both results on hub vibratory loads and vehicle vibration indices demonstrate that an IBC actuation with any harmonics (single or multiple) can be used to decrease the vibration. Specifically, a multi-harmonic IBC with the combined 2P and 4P inputs is the most efficient in reducing the vibration at both the rotor and the pilot seat positions. The reduction is amounted to be about 76.6% for the vertical hub force (F_Z) and 80.6% for the overall vehicle vibration ($VI_{overall}$), as compared with the uncontrolled case. In general, about 10% more reduction in the vibration level is achieved using the multiple harmonic actuation.

Fig. 15 presents the representative IBC actuation signals which showed the best vibration reduction gains (see Fig. 14), respectively for 3P single and combined 2P and 4P multi-harmonic inputs. Comparing the waveforms of the two best harmonic inputs, there is a clear down-up pitch application in the first quadrant and a reversion of up-down trend in the second quadrant of the rotor disk, for both actuation cases. This harmonized behavior of the two signals is observed only in the advancing side, with no consistent waveforms in the retreating side. Note that the retreating side of the rotor disk plays less significant roles in generating the lift for a coaxial L.O. rotor than conventional helicopter rotors. The actuation profiles shown in Fig. 15 and their driving mechanism in reduction the vibration of the aircraft are explained further illustrating the section normal force in contour format. Fig. 16 compares the section normal force distribution between the baseline (uncontrolled) and the best actuation cases, with a time step size of 15°. With the actuation (combined 2P and 4P), the section airloads are substantially redistributed, particularly in the advancing side of the rotor disk. The peak values originally situated in either 30° or 160° zones are shifted more toward 90° azimuth regions due to the active application of pitch input scenarios. The peak amplitudes also become decreased slightly by the actuation process. In summary, the substantial redistribution and decreased peaks in section normal force signals contribute to reduce the vibration levels of the coaxial L.O. rotorcraft in high-speed cruise flight.

4. CONCLUSIONS

In this work, a comprehensive vibration reduction study was performed for an integrated rotor-body system of XH-59A using individual blade pitch control (IBC) technique. A 1D FE stick model of the fuselage was developed based on the natural frequency data of XH-59A and other conventional helicopters. Either one-way or two-way coupled vibration model was employed for the rotorcraft vibration analysis, and its effectiveness was evaluated considering the predicted vibration levels obtained at the rotor hub and pilot seat locations, as compared with the flight test data. The following conclusions were drawn from the study:

1. The fuselage vibration level predicted at the pilot seat of the aircraft was found to be very sensitive to the fuselage vibration modes, especially with the longitudinal and vertical vibrations. The parametric study demonstrated that at least the first fourteen normal modes of the fuselage were needed to reach a sufficient convergence.
2. The iterative two-way rotor-body coupling was shown to significantly improve the correlation with the test data for both the longitudinal and vertical vibration at the pilot seat with the penalty of increased computational costs (20 min vs. 52 min), as compared with the one-way coupled method.
3. The comparison of blade loads (FBM) and vibratory hub moments in reference to the flight test revealed that a L.O. value of 0.2 correctly predicted the general trend of the measured data of the rotorcraft in flight.
4. The influence of the fuselage on the rotorcraft vibration of the L.O. coaxial rotor was indicated to be crucial on the vibratory longitudinal force signal, despite the seemingly small difference (3.7%) on the overall hub vibration level described in index form (VI_R).
5. An IBC actuation with different harmonics was successfully demonstrated for the reduction of vibration at both the rotor hub and the pilot seat locations. The best vibration gains achieved were 67% for a single harmonic actuation at 3P frequency with the amplitudes of 1° and the phase angle of 240°, and 80.6% for multiple harmonic actuation at a combined 2P and 4P frequencies. Phase shifting toward 90° azimuth zones and alleviating the peak magnitudes of the section normal forces were attributed to the sources of the reduced vibration.

Author contact:

Seong Hyun Hong shsky0721@konkuk.ac.kr

Dong Kyun Kim sncs1996@konkuk.ac.kr

Sung Nam Jung snjung@konkuk.ac.kr

5. ACKNOWLEDGMENTSREFERENCES

This work was supported by Korea Research Institute for defense Technology planning and advancement (KRIT) grant funded by the Korea government (DAPA (Defense Acquisition Program Administration)) (No. KRIT-CT-22-082, Design / Manufacturing Technology of Rigid Coaxial Rotor System for High-Speed Compound Helicopter, 2023). This work was supported by the National Research Foundation of Korea (NRF) grant funded by the Korean government (MSIT) (2022R1A4A1018884).

6. REFERENCES

1. Ruddell, A. J., "Advancing blade concept (ABC) technology demonstrator," US Army Research and Technology Laboratories, USAAVRADCOM-TR-81-D-5, 1981.

2. Ruddell, A. J. “Advancing Blade Concept (ABC™) Development,” *Journal of American Helicopter Society,* May 1977

3. Yeo, H., Chopra, I., Coupled Rotor/Fuselage Vibration Analysis Using Detailed 3-D Airframe Models, *Mathematical and Computer Modeling,* 33 (10-11) (2001) 1035-1054.

4. Yeo, H., Chopra, I., “Coupled Rotor/Fuselage Vibration Analysis for Teetering Rotor and Test data Comparison,” *Journal of Aircraft*, Vol. 38, (1) (January-February 2001)

5. Rex, W., Pflumm, T., M. Hajek, “UH-60A Rotor and Coupled Rotor-fuselage Simulation Framework Validation and Analysis,” 45th European Rotorcraft Forum, Warsaw, Poland, Sep 2019.

6. Jacobellis, G., Gandhi, F., and Floros, M., A Physics-Based Approach to Trim Optimization of Coaxial Helicopters in High-Speed Flight, American Helicopter Society 71st Annual Forum Proceedings, Virginia Beach, USA, May 5-7, 2015.

7. Ho, J. C., and Yeo, H.S., "Analytical Study of an Isolated Coaxial Rotor System with Lift Offset", *Aerospace Science and Technology*, Vol. 100, 2020, Paper No. 105818.

8. Lim, J. H., Shin, S. S., and Kee, Y. J., “Optimization of Rotor Structural Design in Compound Rotorcraft with Lift Offset,” *Journal of American Helicopter Society,* Vol. 61, No. 1, pp. 1-14, 2016.

9. Lim, J. W., McAlister, K. W., and Johnson, W., “Hover Performance Correlation for Full-Scale and Model-Scale Coaxial Rotors,” *Journal of American Helicopter Society,* Vol. 54, No. 3, 2009.

10. Schmaus, J., and Chopra, I., Aeromechanics for a High Advance Ratio Coaxial Rotor, American Helicopter Society, 71th Annual Forum Proceedings, Virginia Beach, USA, May 5-7, 2015.

11. Cameron, C. G., Sirohi, J., Schmaus J. and Chopra, I., “Performance and Loads of a Rduced-Scale Coaxial Counterrotating Rotor,” *Journal of American Helicopter Society,*” Vol. 64, No. 4, pp. 1-15, 2019.

12. Cameron, C. G., and Sirohi, J., "Performance and Loads of a Lift Offset Rotor: Hover and Wind Tunnel Testing," *Journal of the American Helicopter Society*, Vol 64, No. 2, pp. 1-12, 2019.

13. Feil, R., Hajek, M., and Rauleder, J., “Vibratory Load Predictions of a High-Advance-Ratio Rotor System Validated by Wind Tunnel Tests,” *Journal of Fluids and Structures*, Vol. 92, 2020, Paper No. 102764.

14. Blackwell, R., and Millott, T., "Dynamic Design Characteristics of the Sikorsky X2 Technology Demonstrator Aircraft," American Helicopter Society 64th Annual Forum Proceedings, Montreal, Canada, Apr. 29-May 1, 2008.

15. Lee, Y. -L, Kim, D. -H., Park, J. -S., and Hong, S. -B., “Vibration Reduction Simulations of a Lift-offset Compound Helicopter Using Two Active Control Techniques,” *Aerospace Science and Technology*, Vol. 106, 2020.

16. Howland, G. R., Durno, J.A., and Twomey, W. J., “Ground Shake Test of the UH-60A Helicopter Airframe and Comparison with NASTRAN Finite Element Model Predictions,” NASA-CR-181993, March 1990.

17. Stoppel, J., Degener, M., “Investigation of Helicopter Structural Dynamics and a Comparison with Ground Vibration Tests,” *Journal of the American Helciopter Society*, Vol. 27, (2), April 1982.

18. Hanson, H. W., “Investigation of Vibration Reduction Through Structural Optimization, US Army Research and Technology Laboratories,” USAAVRADCOM-TR-80-D-13, July 1980.

19. Ruddell, A. J., “XH-59A ABC Technology Demonstrator Altitude Expansion and Operational Tests,” US Army Research and Technology Laboratories, USAAVRADCOM-TR-81-D-35, Dec. 1981.

20. Johnson, W., “CAMRAD II: Comprehensive Analytical Model of Rotorcraft Aerodynamics and Dynamics,” Johnson Aeronautics, Palo Alto, CA, 1992.

21. Heffernan, R., Precetti, D. and Johnson, W., 1991. “Vibration analysis of the SA349/2 helicopter,” No. NAS 1.15: 102794 Jan, 1991.

22. Anonymous, “Standard, Aeronautical Design Standard practice: Requirements for rotorcraft vibration specifications, modeling, and testing,” ADS-27A-SP, US Army Aviation and Missile Command, Redstone Arsenal, Alabama, 2006.

23. Ruddell, A. J., Macrino, J. A., “Advancing Blade Concept (ABC)™ High Speed Development,” American Helicopter Society, Washington, D.C., May, 1980.

Table 1: General properties of XH-59A rotorcraft.

Property	Value
Number of blades, N_b	3
Number of rotors	2
Radius, R	5.48 m
Root cutout	0.2 R
Mean chord, c	0.36 m
Solidity (single rotor), σ	0.064
Hover tip Mach number, M_{tip}	0.58
Fuselage length	12.4 m
Vehicle weight, W_0	5,398 kg
Nominal rotor speed, Ω_0	344 RPM
Cruise mode rotor speed	338 RPM

Table 2: Comparison of natural frequencies for the target fuselage model.

Fuselage mode	Target, Hz	Present, Hz
1st pylon yaw	3.01	3.01
1st pylon pitch	3.90	3.78
1st vertical bending	5.52 - 7.94	6.28
1st lateral bending	5.58 - 7.14	7.6
2nd vertical bending	16.2	16.2
2nd lateral bending	15.3 - 25.2	16.7

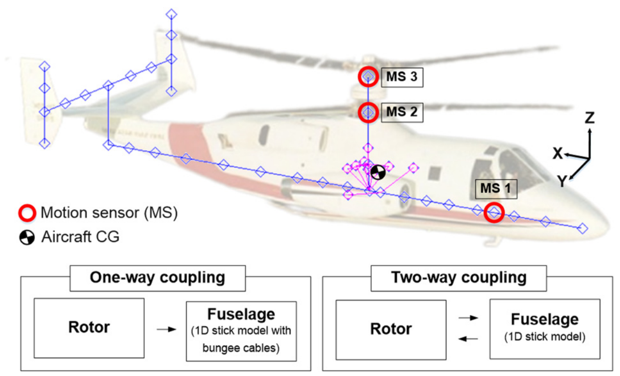

Figure 1. Rotor-body coupled vibration analysis model of XH-59A.

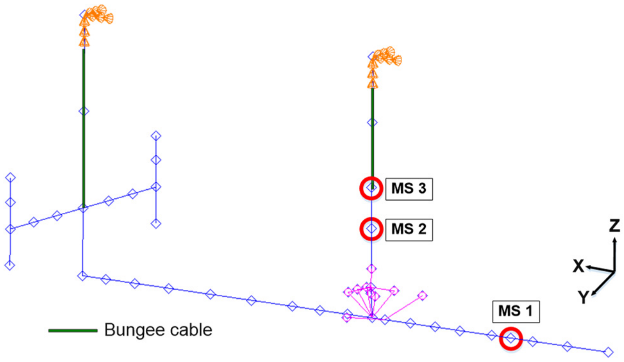

Figure 2. 1D ground vibration analysis model of the fuselage.

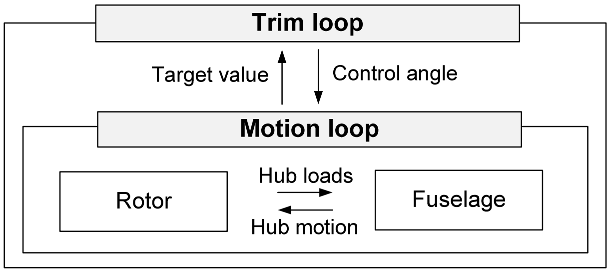

Figure 3. Schematic view of two-way coupled vibration analysis in CAMRAD II (Ref. 20).

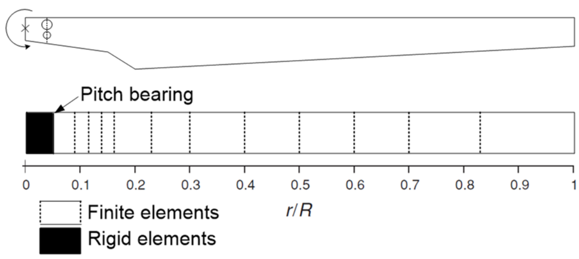

(a) Structural model

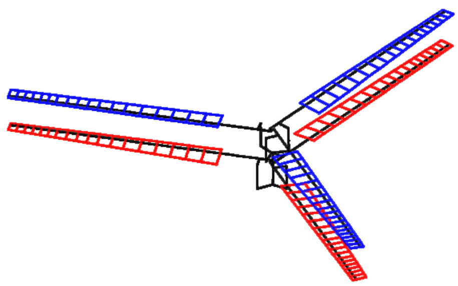

(b) Aerodynamic model

Figure 4. Aeromechanics analysis models of co-axial XH-59A rotor.

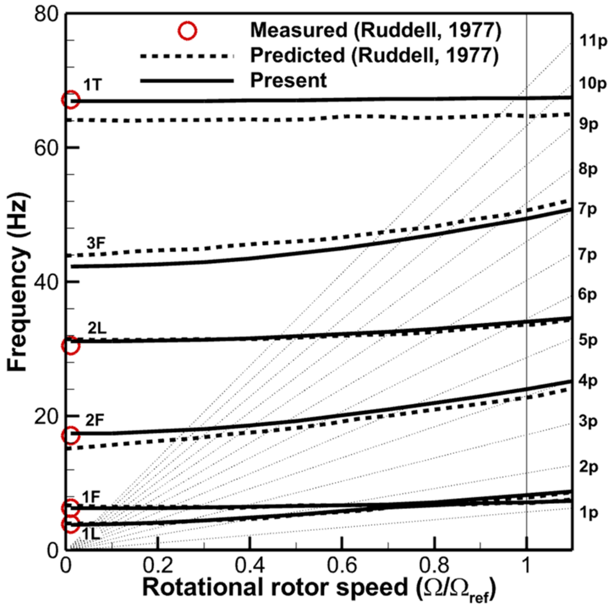

Figure 5. Comparison of rotating natural frequencies.

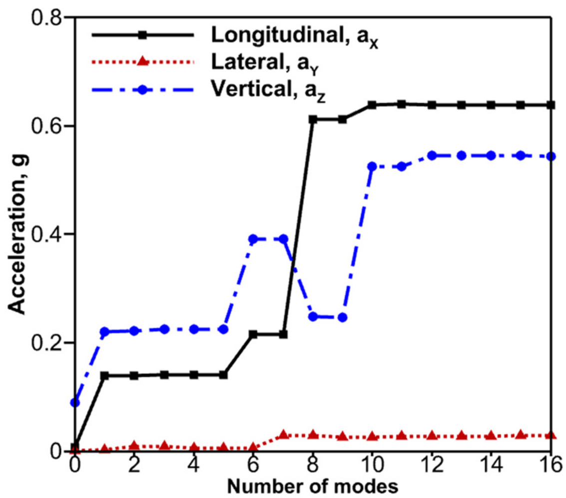

Figure 6. Convergence behavior on fuselage accelerations at the pilot seat (MS 1).

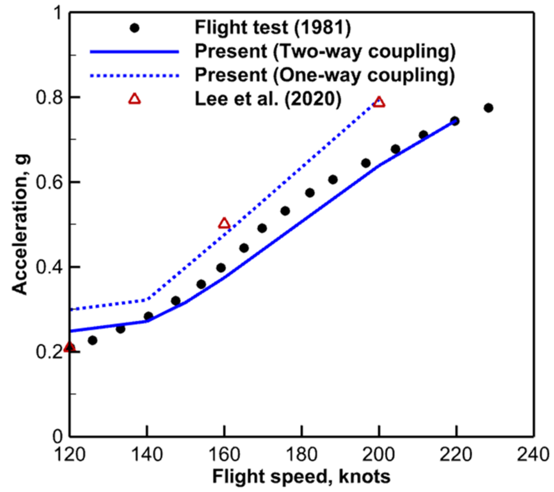

(a) Longitudinal acceleration (a_X)

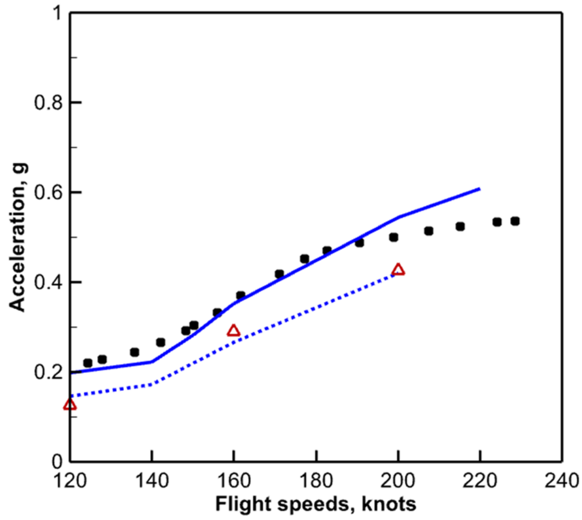

(b) Vertical acceleration (a_Z)

Figure 7. Comparison of fuselage vibration results at the pilot seat (MS 1).

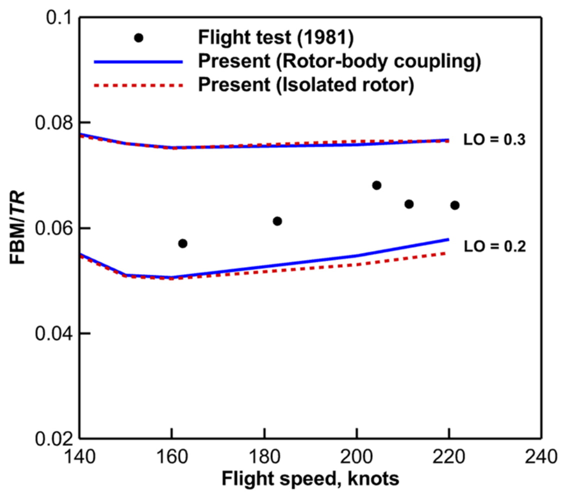

Figure 8. Comparison of flap bending moments (p-p) at the blade root (upper rotor).

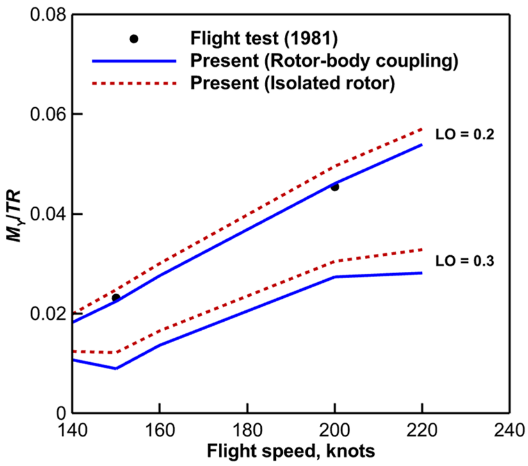

Figure 9. Comparison of vibratory hub pitching moments.

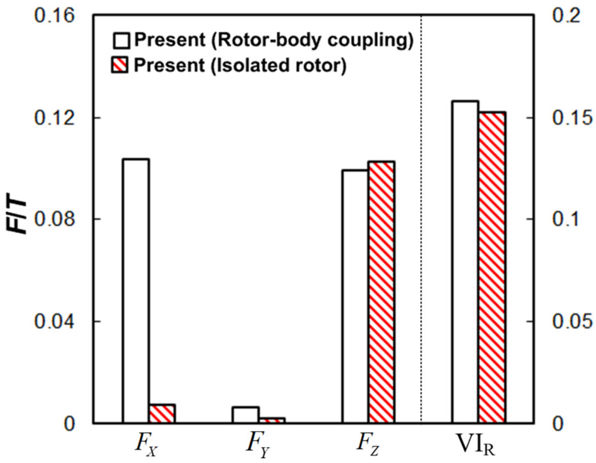

Figure 10. Comparison of vibratory hub loads (L.O. = 0.2).

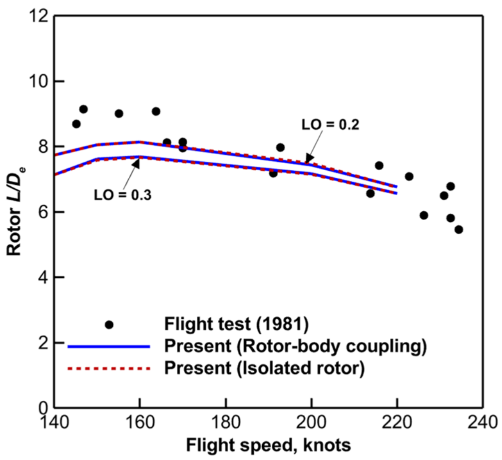

Figure 11. Comparison of rotor effective lift-to-drag ratios.

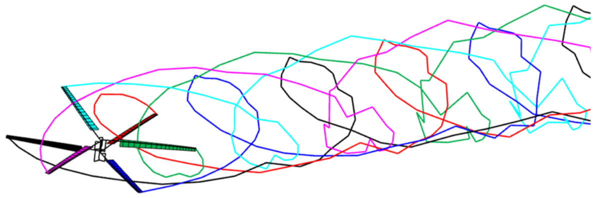

Figure 12. Computed free wake geometry of the coaxial rotor model (μ = 0.53).

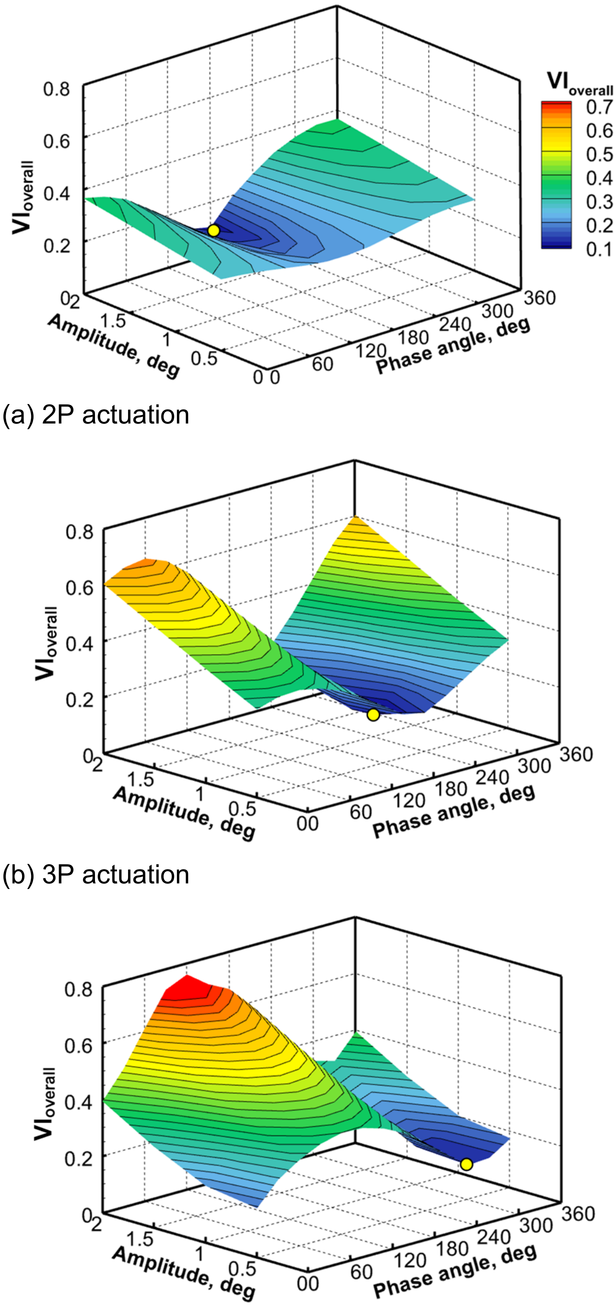

(a) 2P actuation

(b) 3P actuation

(c) 4P actuation

Figure 13. Variation of $VI_{overall}$ due to IBC amplitude/phase sweep of the rotor.

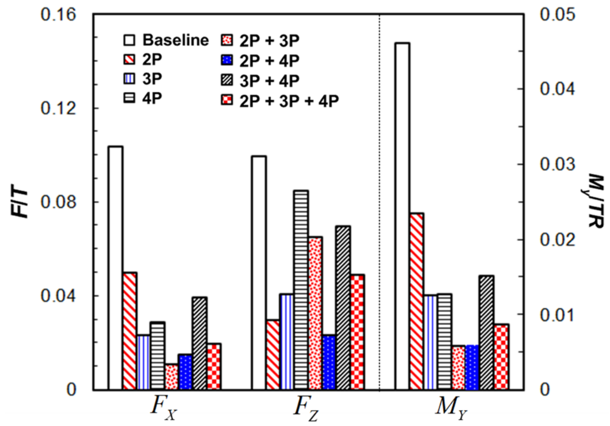

(a) Nondimensionalized hub loads

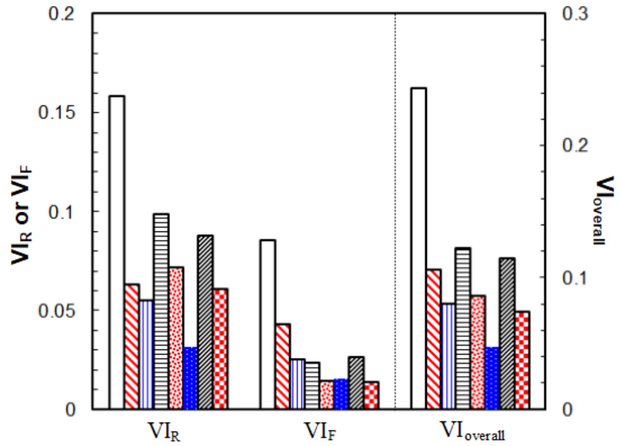

(b) Vibration indexes

Figure 14. Minimum vibration results with respect to IBC actuation scenarios.

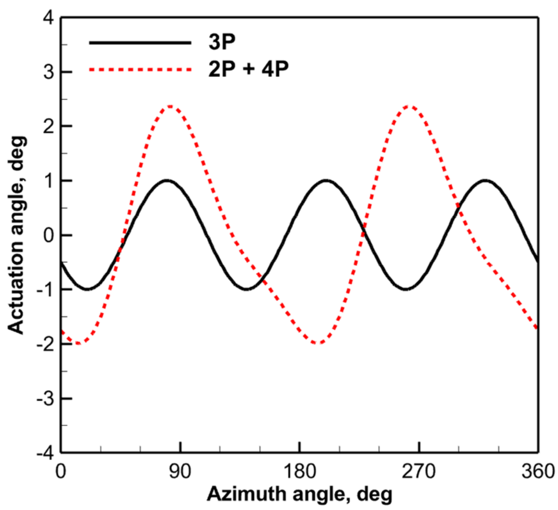

Figure 15. Selected optimal actuation scenarios for vibration reduction.

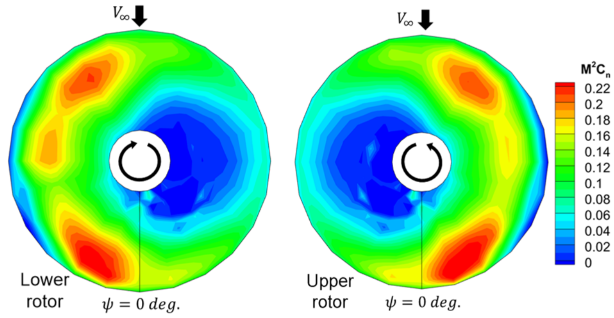

(a) Baseline (uncontrolled)

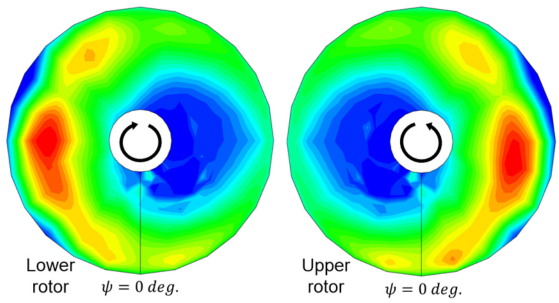

(b) Optimal (2P + 4P)

Figure 16. Comparison of contour plots on section normal force distribution over the rotor disk.